Magnetic hysteresis in small-grained Co_xPd_{1-x} nanowire arrays

M.S Viqueira, G. Pozo-López, S.E Urreta, A.M Condó, D.R Cornejo, L.M Fabietti

www.elsevier.com/locate/jmmm

PII: S0304-8853(15)30245-6
DOI: http://dx.doi.org/10.1016/j.jmmm.2015.06.033
Reference: MAGMA60305

To appear in: *Journal of Magnetism and Magnetic Materials*

Received date: 19 December 2014
Revised date: 3 June 2015
Accepted date: 15 June 2015

Cite this article as: M.S Viqueira, G. Pozo-López, S.E Urreta, A.M Condó, D.R Cornejo and L.M Fabietti, Magnetic hysteresis in small-grained Co_xPd_{1-x} nanowire arrays, *Journal of Magnetism and Magnetic Materials,* http://dx.doi.org/10.1016/j.jmmm.2015.06.033

Magnetic hysteresis in small-grained Co_xPd_{1-x} nanowire arrays

M S Viqueira[1,2], G Pozo-López[1,2,3], S E Urreta[1,], A M Condó[3,4], D R Cornejo[5] and L M Fabietti[1,2,3]

[1] Facultad de Matemática, Astronomía y Física, Universidad Nacional de Córdoba. Ciudad Universitaria, 5000, Córdoba, Argentina.

[2] Instituto de Física Enrique Gaviola – CONICET.

[3] Consejo Nacional de Investigaciones Científicas y Técnicas (CONICET). Argentina.

[4] Centro Atómico Bariloche, Comisión Nacional de Energía Atómica – Instituto Balseiro, Universidad Nacional de Cuyo. Av. Bustillo 9500, 8400, San Carlos de Bariloche, Argentina.

[5] Instituto de Física, Universidade de São Paulo, 05508-900 São Paulo, SP, Brazil.

*Author to whom correspondence should be addressed: S. E. Urreta. urreta@famaf.unc.edu.ar.

Abstract

Co-Pd nanowires with small grain size are fabricated by AC electrodeposition into hexagonally ordered alumina pores, 20-35 nm in diameter and about 1 m long. The effects of the alloy composition, the nanowire diameter and the grain size on the hysteresis properties are considered. X-ray diffraction indicates that the nanowires are single phase, a *fcc* Co-Pd solid solution; electron microscopy results show that they are polycrystalline, with randomly oriented grains (7-12 nm), smaller than the wire diameter. Nanowire arrays are ferromagnetic, with an easy magnetization axis parallel to the nanowire long axis. Both, the coercive field and the loop squareness monotonously increase with the Co content and with the grain size, but no clear correlation with the wire diameter is found. The Co and Co-rich nanowire arrays exhibit coercive fields and reduced remanence values quite insensitive to temperature in the range 4K-300K; on the contrary, in Pd-rich nanowires both magnitudes are smaller and they largely increase during cooling below 100 K. These behaviors are systematized by considering the strong dependences displayed by the magneto-crystalline anisotropy and the saturation magnetostriction on composition and temperature. At low temperatures the effective anisotropy value and the domain-wall width to grain size ratio drastically change, promoting less cooperative and harder nucleation modes.

PACS: 75.75.Cd Fabrication of magnetic nanostructures; 75.75.-c Magnetic properties of nanostructures; 75.30.Gw Magnetic anisotropy; 75.60.Jk Magnetization reversal mechanisms.

Keywords: Co-Pd polycrystalline nanowires; AC electrodeposition; magnetization mechanism; cooperative nucleation mode.

1. Introduction

Magnetic nanowires are interesting nanostructures not only from basic research viewpoints but also because of their applications in data storage [1,2], in gas [3] and acoustic [4] sensor technologies and in modern logic and spintronic devices [5,6].

Ordered arrays of these magnetic nanowires, deposited in self-assembled templates, are also model systems to investigate the magnetization reversal mechanisms in low-dimensional magnetic structures, providing at the same time a valuable insight into the magnetic interaction processes in the periodic array. These phenomena are key factors governing the hysteresis behavior, often limiting the magnetic performance of these materials in many applications.

After Masuda and Fukuda reported the process to obtain highly ordered anodic aluminum oxide (AAO) templates [7] they were widely used to prepare various metal nanowire arrays, as they provide a hexagonal array of about 10^{10} cm^{-2} cylindrical pores, 10 nm to 500 nm in diameter and tens of microns in length where ordered arrays of cylindrical nanowires may be electrodeposited.

Nanowire arrays based on Co-Pd alloys are attractive systems with special properties; in a wide interval including room temperature, these alloys are a continuous series of random substitutional solid solutions with *fcc* structure. Pd addition is found to stabilize the *fcc* Co against the *hcp* Co phase, even at very low concentrations. A second property of the alloying element Pd is that although it is not ferromagnetic, the exchange interaction between the Co (localized) 3d electrons and the 4d electrons of Pd polarizes these later atoms when they are near the Co atom [8]. As a consequence, the moment associated with one Cobalt atom when Co concentration approaches zero is about 9-10 μ_B (Bohr magnetons) while it is about 1.7 μ_B for pure Co. The effect of adding small Pd amounts is then to enhance the spontaneous magnetization and so the shape anisotropy. In the low Co content limit, this phenomenon leads to weak ferromagnetic, Pd-rich nanowires which may be used in the catalysis of useful reactions and also in sensing devices [9].

The magnetization reversal mechanisms in ferromagnetic nanowires have received special attention [10-18]; isolated soft magnetic nanowires, separated from the template by dissolving the membranes using chemical etching, are expected to exhibit quite square hysteresis loops [10], arising in the abrupt

reversal of the magnetization between the two possible remanent states. However, the hysteresis of a macroscopic nanowire array exhibits non-square loops as a result of both, size and shape distributions in the sample, and also due to magnetic interactions between nanowires [19-23]. In fact, the competition between the effective anisotropy field of individual nanowires, and the dipolar interaction fields of the array as a whole, determines the hysteresis loop shape. The dipolar coupling between wires may be described in a mean field approximation by an additional uniaxial anisotropy favoring an in-plane easy axis [19,22]; for planar, regular arrays of magnetic nanowires this dipolar demagnetizing field becomes $\mu_0 H_{dip} = - P J_S$, with J_S the saturation polarization and P the template porosity.

Two de-localized switching modes –coherent rotation and curling – are mainly considered in short, single crystalline uniform wires with quite low aspect ratios, while localized magnetization reversal modes are predicted for long and wide nanowires [11,12]. In cylindrical long and uniform structures, the magnetization reversal is proposed to be driven by the nucleation and propagation of domain walls [10,16-18]; depending on the radius and on the nanowire material, the magnetization reversal may proceed by the propagation of a vortex domain wall or a transverse wall, with these walls moving at very high velocities along the wires. If a single crystalline wire is thin enough, the exchange interaction forces make the magnetization remain homogeneous through any radial cross section of the wire, and the propagation of a transverse wall results the preferred mode for magnetization reversal. These models involving nucleation and further expansion of a single, ideal domain wall through the wires may be rigorously applied to single crystalline wires and perhaps to individual grains in cases where the mean grain size is quite large as compared with the domain wall size and the wire diameter.

Localization is a highly probable phenomenon caused by morphological inhomogenities; in polycrystalline wires defects like grain boundaries, fluctuations in the wire thickness, atomic defects, grain misalignment and/or geometrical features at the wire ends promote strong localization of the nucleation mode [11,12]. In addition, in wires with low saturation magnetization and a small grain size the competition between interatomic exchange and anisotropy may also produce random-anisotropy effects, further reducing coercivity.

Co-rich Co-Pd nanowires have been synthesized in AAO templates by DC [24-27] and AC [28] electrodeposition techniques; the main results reported indicate that the arrays are ferromagnetic, with an easy magnetization axis parallel to the wire length (that is, out of the alumina substrate plane); for small and medium Pd contents both, the coercivity and the reduced remanence or squareness *S* *(=J_R/J_s),* decrease. However, little is known about Pd-rich nanowire arrays.

The relationship between nanostructure and magnetic properties in Co-Pd nanowire arrays, and especially in those produced by AC electrodeposition, has been not much explored [28] and no data is available concerning the actual magnetization reversal mechanisms operating in these quite small grained polycrystalline nanowires.

In this article the microstructure and the magnetic hysteresis properties of Pd-rich Co_xPd_{1-x} nanowire arrays, obtained by AC electrodeposition, are further described in relation to the alloy composition, the nanowire size and geometry, the mean grain size and temperature between 4K and 300K.

2. Experimental procedure

nanowires with different diameters and compositions were prepared by electrodepositing the metal ions within the pores of an anodized aluminum oxide (AAO) membrane; these membranes acting as hard templates exhibit a hexagonal array of pores, quite uniform in diameter and length. Porous AAO templates were prepared, by a two-step anodizing process on high purity (99.995%) aluminum foils in a 0.3 M oxalic acid solution at 276 K, by varying DC voltage between 20 and 40 V. Prior to the anodizing process the foil was degreased and electropolished. In these conditions, pore diameters between 20 nm and 35 nm and lengths of about 1-2 m are obtained. The template porosity *P* and the pore density are estimated [29] as $P = (\pi/2\sqrt{3})(D/D_{\text{int}})^2$ and $\rho = 10^{14}/(\sqrt{3}\, D_{\text{int}}^2)$ respectively, with D the nanowire diameter and D_{int} the mean centre to centre inter-pore distance in the array. The resulting values are included in Table 1; it is worth to note that all the samples exhibit similar $P = (0.11 \pm 0.01)$ in good agreement with the ten%-porosity law [29].

The electrodeposition of Co-Pd nanowires with different compositions was carried out in aqueous electrolytic baths with different proportions of $CoCl_2$ and $PdCl_2$, containing variable relations of Co^{2+}

and Pd^{2+} ions, and 30 g/l of H_3BO_4 included to enhance conductivity. The pH value was adjusted to 5 by adding a few drops of dilute HCl or diluted NH_4OH. The electrodeposition of Co-Pd nanowires was conducted at room temperature under a sinusoidal wave of 200 Hz and 25 V_{rms}, during a few minutes; a two electrode electrochemical cell was used, where the remaining aluminum film in the AAO template served as a working electrode and a graphite rod as an auxiliary one.

The morphology and microstructure of the resulting samples were investigated by scanning electron microscopy (SEM) in a FE-SEM Σigma Zeiss device, and by X-ray diffraction techniques in a Philips PW 3830 X-ray diffractometer with Cu K radiation (λ = 1.5418 Å), in the 2θ range between 30º and 90º, in the Bragg-Brentano configuration. Samples for XRD measurements were prepared by dissolving the remaining Al substrate in a $CuSO_4$ and HCl solution, while for SEM observation the nanowires were further liberated from the template by dissolving the alumina membrane with aqueous 1M Na (OH). When possible, the mean crystallite size of the nanowires was estimated using the Scherrer formula [30].

The nanowire composition was determined for each sample by EDS techniques in a JEOL JXA-8230 equipment. The wire nanostructure was investigated by transmission electron microscopy (TEM) in a Philips CM200UT microscope, operating at 200 kV. Samples for TEM observations were prepared by dispersing the liberated nanowires in ethanol and further depositing a drop of this 6emulsion on a holey carbon-coated copper grid.

The magnetic properties were characterized by measuring the hysteresis loops at two different relative orientations between the sample and the applied magnetic field: = 0º (PA, with the magnetic field parallel to the long nanowire axis) and = 90º (PE, with the magnetic field perpendicular to the long nanowire axis). Room temperature magnetic hysteresis loops were performed in a Lakeshore 7300 vibrating sample magnetometer with a maximum field up to 1.5 T; samples with low magnetization signals were measured in a MPMS Quantum Design Squid (*Superconducting Quantum Interference Device*) magnetometer in the temperature range between 5 K and 300 K.

The total magnetic moment of the assembly has contributions from the Al support (paramagnetic), the alumina template (diamagnetic) and the metallic wires filling the pores (ferromagnetic) so in low-

signal arrays (for example Co11 samples) the ferromagnetic component must be estimated after subtracting a linear contribution.

The different arrays are named CoX-Y, with X the Cobalt composition in at.% and Y the nominal mean wire diameter in nanometers.

3. Results and Discussion

3.1. Morphology and structure

The alumina templates are illustrated in Figure 1.a (top view) and 1.b (side view); they are about 1-2 μm thick and depending on the anodizing voltage, pore diameters between 20 nm and 35 nm are obtained. These cylindrical pores are ordered in the short range scale; depending on the anodizing voltage and the electrolyte used, these AAO templates exhibit pores hexagonally ordered in 'domains' or 'grains', typically 0.3-1 micron in size. Figure 1 corresponds to a central sector of one of these 'order domains' of about 1 m^2, in a 26 nm diameter template, grown in oxalic acid at 25V. This hexagonal order and the pore size uniformity deteriorate when the anodizing voltage is reduced below the optimum self assembling value of 40 V for oxalic acid. Figure 1.c shows a top view of a 26 nm diameter template, showing the pores filled with metallic $Co_{11}Pd_{89}$ nanowires (zone A) and Figure 1.d shows a complete view of these nanowires, both after the removal of the Al support and a partial dissolution of the alumina template. Based on similar images, the inter-pore distance, the pore wall thickness and the wire mean diameter and length are estimated, together with the mean aspect ratio ($a_r = \frac{D}{L}$) of the array, which reached in all the cases values between 20 and 40.

It is found - see Table 1 - that the nanowire diameter is somewhat smaller than the pore diameter, as determined from SEM micrographs, and this fact is further confirmed by TEM observations as will be shown later. The wire mean length is controlled by the electrodeposition time and values of (1.0±0.2) μm are obtained.

X-ray diffraction patterns corresponding to arrays Co11-20, Co11-32 and Co60-32, measured after removal of the aluminum substrate, are shown in Figure 2. The narrow peak at 31.66º corresponds to the polystyrene layer (JCPDS card no. 00-0130836) deposited onto the alumina membranes to

improve their mechanical resistance. Based on the metallic Palladium data (JCPDS card no. 00-046-1043), the peaks at 40.12º and 46.66º are indexed as the (111) and the (200) peaks of *fcc* PdCo alloys. These peaks are broad and very difficult to detect, as in sample Co11-20, because of a quite small crystallite size, as discussed below. In this figure the pattern corresponding to Co nanowires, Co100-32, exhibiting a marked (001) hexagonal texture is also shown as reference.

The average crystallite diameter d of the Co-Pd phase in samples shown in Figure 2 are roughly estimated using the Scherrer equation [30] for the (111) and (200) reflections: $d = (0.9\,\lambda)/(\beta\cos\theta)$, with β (in radians) the peak intrinsic breadth after subtraction of the instrumental contribution, λ the X-ray wavelength and θ the Bragg angle. The resulting values, which correspond to a coherence length along the wire axis, are d = (15 5) nm for Co11-20, d = (20 5) nm for Co11-32, d = (25 5) nm for Co60-32 and d = (42 10) nm for Co100-32, respectively; it is then concluded that this procedure is not adequate to estimate any difference in the grain size between wires with different diameters and/or compositions. These correlations are then examined with TEM techniques.

The morphology and structure of Pd rich nanowires were further explored with TEM and the results corresponding to samples Co11-20, Co11-32 and Co11-35 are displayed in Figure 3 to Figure 5, respectively. Figure 3 shows a bright field (BF) TEM micrograph of Co11-20 nanowires in (a), and the corresponding 111 dark field (DF) image in (b), to evidence the nanowire internal structure. The selected area electron diffraction (SAED) pattern is presented in (c). Figures 3.d and 3.e show the nanowire diameter distribution and the grain size distribution in the sample, also obtained by TEM. Similar micrographs were taken for samples Co11-32 and Co11-35 and the corresponding histograms were also measured; these results are displayed in Figures 4 and 5, respectively.

Table 1. Mean nanowire diameter $\bar{D}$ and the corresponding standard deviation $_D$ listed together with the mean grain size $\langle d \rangle$ and $_d$ estimated by fitting the grain size histograms by a lognormal distribution (correlation factor $r^2 > 0.99$). Details of the ordered arrays as the mean inter-pore distance D_{int}, the nominal porosity P and the nominal pore density are also included.

Sample	$\bar{D}$ [nm]	$_D$ [nm]	<*d*> [nm]	$_d$ [nm]	D_{int} [nm]	*P* [%]	10^{10} cm^{-2}
Co11-20	20	5	11.0	0.4	60	10.8	2.79
Co11-26	21	5	8.5	0.5	73	11.3	1.85
Co11-32	33	8	10.5	0.5	92	10.4	1.43
Co11-35	33	10	12.5	0.5	101	11.4	1.19
Co23-26	18	5	11.5	0.5	73	11.0	0.98

The mean grain sizes of samples with different diameters and compositions, obtained by fitting a lognormal function to the histograms measured by TEM, are summarized in Table 1. As previously observed, the electrodeposited nanowires are polycrystalline, with mean grain size values smaller than the wire diameter, so perfect "bamboo-like" grain structures are excluded. The small grains are equiaxed and randomly oriented; Pd addition to Co wires reduces the grain size but no clear correlation could be established with the alloy composition. Electron diffraction patterns confirm that the only phase in the wires is a *fcc* Pd-Co alloy, in agreement with XRD results. The relatively small and broad XRD peaks measured for these nanowires are then explained by the quite small grain size of this phase, almost in the detection limit of this technique. Finally, the nanowire surface in Co-rich samples is frequently irregular and in some cases, the wires exhibit severe fluctuations in diameter; Pd-rich wires, on the other hand, have relatively smooth surfaces and quite constant diameter along the wire length.

3.2. *Room temperature magnetic properties*

Nanowires are ferromagnetic; the room temperature hysteresis loops of the arrays, measured with the applied magnetic field parallel (PA) and perpendicular (PE) to the wire long axis, are shown in Figure 6 for two nanowire arrays with similar wire diameter but different compositions. In the sample with high Co content, measured in the PA configuration, the saturating field, the coercive field and the remanent magnetic moment are larger, indicating that this is an easy magnetization direction in the

array, that is, there is an easy magnetization axis perpendicular to (out of plane) the Al substrate foil and parallel to the nanowire length. This phenomenon is observed in a more or less extent in all the arrays investigated and may be explained on the basis of a large shape anisotropy in the elongated magnetic nanowires, with aspect ratios a_r between 20 and 40. It is more marked in Co-rich arrays while this magnetic anisotropy largely reduces in samples with the lowest Co content ($Co_{11}Pd_{89}$). This effect is further confirmed by the room temperature dependence of the coercive field on the nanowire composition shown in Figure 7 for wires of nominal diameters of 26 nm and 32 nm, respectively. In both cases the coercive field increases with the Co content for the two field configurations used, in agreement with data reported by other authors [28].

Magnetism in dilute solutions of cobalt in palladium has been investigated by Bozorth *et al.* by 1961 [8]; they find ferromagnetism at 291 K for compositions above 8 at. % Co with a saturation polarization near 0.3 T, almost twice that predicted by a mixture rule, and they also report a Curie temperature about 347 K for 11 at.% cobalt. In this way, larger saturation magnetizations also lead to larger shape anisotropy fields values and then, to higher coercivities. The shape anisotropy constant K_S is approximately given by [31]:

$$K_S = \frac{1}{2\mu_0} \Delta N \, J_S^2 \qquad (1)$$

where $\Delta N (= N_\perp - N_\parallel)$ is the difference between the demagnetizing factors corresponding to the perpendicular and parallel direction, respectively and J_S the saturation polarization. Then, the saturating field associated to this shape anisotropy is $\mu_0 H_S = \Delta N \, J_S \cong 0.5 \, J_S$, leading to values near 220 mT, 365 mT, 506 mT, 600 mT and 760 mT for Co contents of 0.11, 0.23, 0.45, 0.60 and 0.80, respectively. These values are upper bounds for a coercive field controlled by shape anisotropy in these samples. The resulting room temperature coercive fields - in the range between 10 mT and 180 mT - are lower but comparable to those reported by Hu et al. [24] (90 mT) in $Co_{30}Pd_{70}$ nanowires, 55 nm in diameter, and to those found by Vega et al. [27] (125 mT) in $Co_{56}Pd_{44}$ nanowires 35 nm in diameter. In these two cases, DC electrodeposition techniques were employed to produce the metallic nanowires; for AC (200 Hz) electrodeposited wires of 55 nm diameter and 1 m long, Ding et al. [28]

found coercive field values about 100 mT for $Co_{30}Pd_{70}$ arrays. Even when all these results are of the same order of magnitude, the large dispersion observed confirms that not only the wire composition but other variables like the wire/array microstructure determine the magnetic hysteresis properties. Finally, the differences between experimental values and those predicted considering different contributions to the effective magnetic anisotropy are certainly due to imperfections, as any disorder gives rise to a localization-related coercivity reduction [12]. In fact, localization originated from polycrystallinity, wire-thickness fluctuations, crystalline defects locally reducing K, grain misalignment or from a combination of these factors may drastically reduce coercivity.

In Co and Co-based nanowire arrays the coercive field is found to increase with the nanowire length in the low aspect ratio range, but it slightly changes above $a_r > 10$ [32,33]. Then, little or no influence of small fluctuations in the wire length on the magnetic hardness is expected in our samples.

It is generally found that coercivity decreases with increasing wire diameter in the range between 8 nm and 500 nm [33,34] and some authors [35] explain this behavior considering that larger diameters promote less uniform magnetization configurations, which largely reduce the critical field for magnetization reversal.

Figure 8 shows the coercive field, as a function of the nanowire diameter, measured with the applied field in PA and PE configurations for pure Co samples and for two Co-Pd arrays with high and low Pd contents. It may be observed that in the restricted range of diameters investigated, no clear dependence of coercivity on the nanowire diameter can be rigorously established.

In all the samples the nanowire diameters satisfy $D \geq D_{coh} = 7.3\sqrt{\mu_0 A / J_S^2}$, with A the exchange stiffness. Depending on the alloy composition D_{coh} is between 15 nm (Co100) and 18 nm (Co11), so *localized* demagnetization modes are favorable [11,12]. This localization and the fact that wires are polycrystalline, lead to a direct correlation between grain size and coercivity for each composition- see Table 1. However, no clear correlation between the grain size and the wire diameter could be rigorously established in this work.

Regarding dipolar interactions between nanowires in the array, they depend on porosity and on the spontaneous polarization, exhibiting values about 45mT in samples Co11 and 180 mT in Co100

nanowires at room temperature; these values are about the 25% of those estimated for the shape anisotropy, of about 219 mT and 887 mT respectively.

3.3. *Temperature dependent hysteresis properties*

The temperature dependence of the coercive field $\mu_0 H_C$ and the squareness factor $S=M_R/M_S$ of the nanowire arrays investigated are shown in Figure 9 and Figure 10.

The properties corresponding to a Co100-32 nanowire array are included in Figure 9 only for comparison with the Pd alloyed nanowires. The coercive field of the array of Co nanowires in both field configurations is practically constant between 300 K and 4 K, as expected for a switching field controlled by the shape anisotropy term; no transition from a shape to crystalline anisotropy controlled coercivity is observed. The loop squareness in the PA configuration slightly decreases while that for the PE direction little increases during cooling, indicating that quite small changes in the effective anisotropy in parallel and perpendicular directions take place during cooling.

Similar curves are shown in Figure 10 for samples Co45-32, Co23-32 and also for the very small-grained Co11-26 array. The behavior of Co45-32 is quite similar to Co100-32 in the sense that coercivity and relative remanence remain almost temperature independent, exhibiting only small slopes of opposite signs. When the Pd content increases above 55 at. %, the coercive field and the squareness become more temperature sensitive, as if larger magnetoelastic and/or magnetocrystalline contributions to the effective anisotropy were present. In fact, the magnetocrystalline anisotropy energy K_1 [36] and the saturation magnetostriction λ_S [36,37] of Co-Pd alloys depend on composition and temperature in a non trivial manner. Both constants are negative and they go through a maximum absolute value between 10-25 at.% Co, and at temperatures below about 100 K. Then, even when at room temperature the shape anisotropy seems to be dominant, other contributions cannot be excluded below room temperature.

At low temperature, a magnetoelastic anisotropy field arises in the thermal expansion mismatch between the aluminum substrate, the alumina template and the metallic nanowires as proposed in [38]. Assuming that the lateral contraction of the alumina template and the reduction of the nanopore diameter are only controlled by the contraction of the Al substrate, the alumina contraction in the

direction PE becomes $\varepsilon^{PE}_{alumina} = \Delta T(\alpha_{Al} - \alpha_{alumina}) = -4.45\times10^{-3}$ ($\alpha_{Al} = 23.8\times10^{-6}$; $\alpha_{alumina} = 6\times10^{-6}$; $\Delta T = -295\ K$). The elongation of the alumina pore becomes then $\varepsilon^{PA}_{alumina} = -\nu\varepsilon^{PE}_{alumina}$ = 1.02 10^{-3} ($_{alumina}$ = 0.23). Because of the mismatch between the Al support and the Co-Pd wire, this later undergoes-an axial extension $\varepsilon^{PA}_{CoPd} = -\nu\varepsilon^{PE}_{CoPd}$ which is slightly smaller than that of the alumina pore. Then, assuming a perfect interface adhesion (keeping the wires attached to the template), an upper limit for the tensile stress is given by: $\sigma^{PA}_{CoPd} = E_{CoPd}\varepsilon^{PA}_{CoPd}$ = 158 MPa (Co11) and 195 MPa (Co45). This stress introduces an extra axial effective field $\mu_0 H^{\sigma}_{CoPd}(4K) = 3\mu_0\lambda_S\sigma^{PA}_{CoPd} / J_S$ = -150 mT (Co11) and -63 mT (Co45), which reduces the shape anisotropy along the nanowire axis. This contribution is small as compared with the shape anisotropy field of Co (900 mT) and Co45 (520 mT) but is closer to that in Co11 (220 mT) nanowires. Figure 11 shows the temperature dependence of the magneto-crystalline $_K$, the magneto-elastic , and the shape $_S$ anisotropy fields, estimated using the data reported in [8, 36, 37] for the temperature and/or composition dependences of the crystalline anisotropy, the saturation magnetostriction, the saturation polarization and the Curie temperature, respectively. The Young modulus and the exchange energy constant A for the different compositions were roughly estimated using the mixture rule.

These strong temperature and composition dependences of the Curie temperature and of the magneto-crystalline energy density induce large changes in the localization length of the nucleation modes [11,12].

3.4. *Magnetization mechanism*

The magnetic microstructure of these arrays must be realized in terms of nanowires formed by fine, exchange coupled particles, agglomerated in a geometry promoting large shape effects, with a relatively random crystalline orientation, and with these contributions competing to determine the array's magnetic configuration.

Regarding the magnetization mechanisms, the chain of spheres model [14], used for template assisted electrodeposited nanowires, assumes that no exchange interactions take place between the

units in the chain, a condition that is not fulfilled in our case, where the mean grain sizes are comparable or smaller than the magnetic domain wall width and the wire diameter in all the Co-Pd samples. As previously discussed, nucleation and expansion of ideal transverse or vortex like walls, sweeping the entire wire length as proposed for single crystalline wires, seems not favorable in polycrystalline nanowires.

In small-grained nanowires, magnetization reversal is likely to initiate in localized regions [10-13], mainly at imperfections, by polarization rotation (coherent or by curling) in a cooperative Stoner-Wohlfarth (SW) unit (grain or exchange coupled agglomerate) under a combined magnetostatic and exchange mean field. Inversion further proceeds by an avalanche/expansion process, in a random-anisotropy media. This cascade should not be in principle too different from the propagation of a domain-wall like spin configuration and a more detailed description of these processes becomes necessary.

In this picture, large changes in coercivity with temperature and composition may be expected when the localization length reduces, promoting non-cooperative harder nucleation modes. These effects arise from a strong temperature and composition dependences of the Curie temperature and the magneto-crystalline energy density in Co-Pd alloys near 10-20 at. % Co.

Regarding the effect of grain size on coercivity and loop squareness, it may be rationalized considering the large decrease in the random crystalline anisotropy of the agglomerates when the number of grains acting cooperatively increases.

4. Conclusions

Co-Pd nanowires with different compositions and diameters have been produced by AC electrodeposition into the hexagonally arranged pores of a self assembled alumina template. The nanowires obtained by this AC method are nanocrystalline, with randomly oriented grains of mean sizes between 7 nm and 12 nm, smaller than the wire diameter. No correlation could be established between grain size and the alloy composition nor with the wire diameter.

Nanowire arrays are ferromagnetic in the entire range between 4 K and 300 K; they all exhibit an easy magnetization axis parallel to the long wire axis (out of the substrate plane) and a hard direction perpendicular to the nanowire length, with no crossover in the temperature ranges investigated.

The coercive field and the relative remanence of the nanowire arrays both increase with the Co content in the alloy and with the grain size. In Pd-rich wires having very small grains, the coercive fields and the relative remanences (in PA and PE configurations) largely increase during cooling below 100K as a result of a drastic reduction of the localization length promoting non-cooperative, harder nucleation modes. These effects arise from a strong temperature and composition dependences of the Curie temperature, the saturation magnetostriction and the magneto-crystalline energy density in Co-Pd alloys near 10-20 at. % Co. Then, grain size and composition are key microstructure factors to explain the temperature dependence of the coercive field and the relative remanence in Pd-rich wires below 100K.

The magnetization reversal initiates, mainly at imperfections, by the local rotation of a cooperative Stoner-Wohlfarth unit (grain or exchange coupled agglomerates) under a combined magnetostatic and exchange mean field; inversion further proceeds by an avalanche process and/or the propagation of domain wall-like spin configurations.

Acknowledgment

The authors wish to thank FONCyT, SECyT-UNC and CONICET Argentina for the financial support given to this work.

References

1. Srivastava, A K, Singh, R S, Sampson, K E, Singh, V P, Ramanujan, R V, Templated assembly of magnetic cobalt nanowire arrays, 2007, *Metal. and Mater. Trans.*, **38**, 717-724.

2. Samardak, A. S., Sukovatitsina, E. V., Ognev, A. V., Chebotkevich, L. A., Mahmoodi, R., Peighambari, S. M., Hosseiniand, M. G., Nasirpouri, F., High-density nickel nanowire arrays for data storage applications, 2012, *J. Phys.: Conf. Ser*. **345**, 012011.

3. Carpena-Núñez, J., Yang, D., Kim, J-W., Park, C., Fonseca, L. F., Mechanical characterization of pristine and hydrogen-exposed palladium nanowires by in situ TEM, 2013, *Nanotechnology* **24** (3), 035701.

4. McGary, P. D., Tan, L., Zou, J., Stadler, B. J. H., Downey, P. R., Flatau, A. B., Magnetic nanowires for acoustic sensors, 2006, *J. of Appl. Phys.* **99** 8, 08B310-316.

5. Nautiyal, T., Rho, T. H., Kim, K. S., Nanowires for spintronics: A study of transition-metal elements of groups 8–10, 2004, *Phys. Rev.* B **69**, 193404.

6. Hrkac, G,. Dean, J. D., Allwood, A., Nanowire spintronics for storage class memories and logic, 2011, *Philos. Trans.* A*: Math. Phys. Eng. Sci.* **369**, 3214-28.

7. Masuda, H., Fukuda, K. S., Ordered Metal Nanohole Arrays Made by a Two-Step Replication of Honeycomb Structures of Anodic Alumina, 1995, *Science* **268**, 1466-1468.

8. Bozorth, R. M., Wolff, P. A., Davis, D. D., Compton, V. B., Wkrnick, J. H., Ferromagnetism in dilute solutions of Cobalt in Palladium, 1961, *Phys. Rev.* **122** (4), 1157-1160.

9. Lewis, F. A., The Palladium-Hydrogen System, a survey of hydride formation and the effects of hydrogen contained within the metal lattices, Platinum Metals Rev., 1982, **26**, (l), 20-27.

10. Hertel, R., Computational micromagnetism of magnetization processes in nickel nanowires, 2002, *J. Magn. Magn. Mater*. **249**, (1–2), 251–256.

11. Skomski, R., Zeng, H., Zheng, M., Sellmyer, D. J., Magnetic localization in transition-metal nanowires, 2000, *Phys. Rev.* B **62**, (6), 3900-3904.

12. Skomski, R., Zeng, H., Sellmyer, D.J., Incoherent magnetization reversal in nanowires, 2002, *J. Magn. Magn. Mater.* **249**, 175–180.

13. Skomski, R., Exact nucleation modes in arrays of magnetic particles**,** 2002, *J. Appl. Phys.* **91**, (10), 15.

14. Jacobs, I. S., Bean, C. P., An Approach to Elongated Fine-Particle Magnets, 1955, *Phys. Rev.* **100** (4) 1060-1067.

15. Aharoni, A., Angular dependence of nucleation by curling in a prolate spheroid, 1997, *J. Appl. Phys.* **82**, 1281.

16. Landeros, P., Allende, S., Escrig, J. Salcedo, E., Altbir, D., Vogel, E. E., Reversal modes in magnetic nanotubes, 2007, *Appl. Phys. Lett.* **90** 102501.

17. Lavín, R., Denardin, J. C., Escrig, J., Altbir, D., Cortés A., Gómez, H., Angular dependence of magnetic properties in Ni nanowire arrays, 2009, *J. Appl. Phys.* **106**, 103903.

18. Lavin, R., Denardin, J. C., Espejo, A. P., Cortés, A., Gómez, H., Magnetic properties of arrays of nanowires: Anisotropy, interactions, and reversal modes, 2010, *J. Appl. Phys.* **107**, 09B504.

19. Encinas-Oropesa, A., Demand, M., Piraux, L., Huynen, I., Ebels, U., 2001, Dipolar interactions in arrays of nickel nanowires studied by ferromagnetic resonance, *Phys. Rev. B* **63**, 104415.

20. Zhan, Qing-Feng, Gao, Jian-Hua, Liang, Ya-Qiong, Di, Na-Li, Cheng, Zhao-Hua, Dipolar interactions in arrays of iron nanowires studied by Mössbauer spectroscopy, 2005, *Phys. Rev.* B **72**, 024428.

21. Zighem, F., Maurer, T., Ott, F., Chaboussant, G., Dipolar interactions in arrays of ferromagnetic nanowires: A micromagnetic study, 2011, *J. Appl. Phys.* **109**, 013910.

22. Xiaoming Kou , Xin Fan , Randy K. Dumas , Qi Lu , Yaping Zhang , Hao Zhu , Xiaokai Zhang , Kai Liu , and John Q. Xiao; Memory Effect in Magnetic Nanowire Arrays, 2011, *Adv. Mater.* **23** 1393–1397.

23. Dmytriiev, O., Al-Jarah, U. A. S., Gangmei, P., Kruglyak, V. V., Hicken R. J., Mahato, B. K., Rana, B., Agrawal, M., Barman, A., M´at´efi-Tempfli, M., Piraux, L., M´at´efi-Tempfli, S., 2013, Static and dynamic magnetic properties of densely packed magnetic nanowire arrays. *Phys. Rev. B* **87**, 174429.

24. Hu, H. N., Chen, H. Y., Yu, S. Y., Chen, L. J.,. Chen, J. L., Wu, G. H., Fabrication and magnetic properties of CoxPd1_x composite nanowire, 2006, *J. Magn. Magn. Mater.* **299**, 170-175.

25. Xu, Cai-Ling, Li, Hua, Xue, Tong, Li, Hu-Lin, Fabrication of CoPd alloy nanowire arrays on an anodic aluminum oxide/Ti/Si substrate and their enhanced magnetic properties, 2006, *Scripta Mater*. **54**, 1605–1609.

26. Vivas, L. G., Vázquez, M., Vega, V., García, J., Rosa, W. O., del Real R. P., Prida, V.M., Temperature dependent magnetization in Co-base nanowire arrays: Role of crystalline anisotropy, 2012, *J. of App. Phys.* **111**, 07A325.

27. Vega, V., Rosa, W.,O., García, J., Sánchez, T., Santos, J. D., Béron, F., Pirota, K. R., Prida, V. M., Hernando, B., Template-Assisted CoPd Nanowire Arrays: Magnetic Properties and FORC Analysis, 2012, *J. of Nanosc. and Nanotech.* **12**, 1–8.

28. Ding, J-B., Qin, D-H., Huang, Y., Cao, L., Li, H-L., Fabrication and magnetic properties of CoPd nanowire arrays, 2003, *J. Mat. Eng. and Performance (JMEPEG)* **12**, 584.

29. Nielsch, K., Choi, J., Schwirn, K., Wehrspohn, R.B. and Gosele, U., Self-ordering Regimes of Porous Alumina: The 10% Porosity Rule, 2002, *Nano Lett*., **2** 677.

30. Patterson, A. L., The Scherrer Formula for X-Ray particle size determination, 1939, *Phys. Rev.* **56**, 15.

31. O'Handley, R. C., Modern Magnetic Materials. Principles and Applications, 2000, John Wiley and Sons. New York.

32. Zeng, H., Zheng, M., Skomski, R., Sellmyer, D. J., Liu, Y., Menon, L., Bandyopadhyay, S., Magnetic properties of self-assembled Co nanowires of varying length and diameter, 2000, *J. App. Phys.* **87**, (9), 4718-4720.

33. Vivas, L. G., Yanes, R., Chubykalo-Fesenko, O., Vazquez, M., Coercivity of ordered arrays of magnetic Co nanowires with controlled variable lengths, 2011, *Appl. Phys. Lett.* **98**, 232507.

34. Piraux, L., Dubois, S., Ferain, E., Legras, R., Ounadjela, K., George, J. M., Maurice, J. L. and A. Fert. Anisotropic transport and magnetic properties of arrays of sub-micron wires, 1997, *J. Magn. Magn. Mater.* **165**, 352-355.

35. Zhang, L., Zhang, Y., Fabrication and magnetic properties of Fe_3O_4 nanowire arrays in different diameters, 2009, *J. Magn. Magn. Mater.* **321** L15–L20.

36. Fujiwara, J . H., Kadomatsu, H., Tokunaga, T., Magnetocrystalline anisotropy and magnetostriction of Pd-Co alloys, 1983, J. Magn. Magn. Mater. **31-34** 809-810.

37. Takahashi, H., Tsunashima, S., Iwata, S., Uchiyama S., Measurement of magnetostriction constants in polycrystalline alloy and multilayer films of PdCo and PtCo,1993, J. Magn. Magn. Mater. **126** 282-284.

38. Sánchez-Barriga, J., Lucas, M., Radu, F., Martin, E., Multigner, M., Marin, P., Hernando, A., Rivero, G., Interplay between the magnetic anisotropy contributions of cobalt nanowires, 2009, *Phys. Rev. B* **80** 184424.

Figure captions

Figure 1. SEM micrographs showing a top view (a) and side view (b) of an alumina template of 26 nm pore diameter, a top view of a template filled by metallic nanowires (c), and nanowires (d), both after the removal of the Al support and a partial dissolution of the alumina template.

Figure 2. XRD patterns corresponding to arrays Co11-20, Co11-32 and Co60-32 after removal of the Al substrate. The diffractogram corresponding to a Co sample is also included. The reflection denoted by P arises from the polystyrene layer added to improve the membrane mechanical resistance. Small Cu crystals, originated in the Al dissolution process are also detected. The PdCo diffraction lines from the nanowires are hardly detected in Pd-rich samples with 20 nm pore diameter.

Figure 3. (a) Bright field (BF) TEM micrographs of Co11-20 nanowires; (b) 111 dark field (DF) image illustrating the nanowire internal structure and (c) selected area electron diffraction pattern (SAEDP) corresponding to the nanowires in (a) and (b). Nanowires are polycrystalline, with a quite small grain size. Histograms corresponding to the wire diameter (d) and the grain size (e) distributions resulting from TEM data are included.

Figure 4. (a) BF TEM micrograph showing Co11-32 nanowires; the corresponding 111 DF image and the SAEDP are shown in (b) and (c) respectively. The polycrystalline nanowire structure is clearly observed. Histograms corresponding to the wire diameter (d) and the grain size (e) distributions are also shown.

Figure 5. BF TEM micrographs showing Co11-35 nanowires (a); the corresponding 111 DF image (b) and the SAEDP (c) indicate that wires are nanocrystalline. Histograms corresponding to the wire diameter (d) and the grain size (e) distributions are also shown.

Figure 6. Room temperature hysteresis loops of samples Co45-32 (a) and Co11-32 (b) measured with the applied field parallel (PA) and perpendicular (PE) to the nanowire major axis. The different loops obtained in these two configurations are consistent with a relatively large shape anisotropy.

Figure 7. Coercive field as a function of the alloy Co content in arrays of 26 nm (circles) and 32 nm (squares) diameter nanowires.

Figure 8. Coercive field as a function of the mean nanowire diameter for arrays with different compositions: pure Co (Co100), $Co_{45}Pd_{55}$ (Co45) and $Co_{11}Pd_{89}$ (Co11). Full symbols correspond to measurements performed with the applied field parallel to the wire long axis while the open ones correspond to the perpendicular configuration.

Figure 9. Temperature dependence of coercivity and squareness in Co nanowire arrays 32 nm in diameter. PA and PE indicate that the magnitude is measured with the magnetic field applied parallel or perpendicular to the nanowire long axis.

Figure10. Temperature dependence of coercivity (a and b) and squareness (c) in nanowire arrays with different compositions. PA and PE indicate that the magnitude is measured with the magnetic field applied parallel or perpendicular to the nanowire long axis.

Figure 11. Temperature dependence of the magneto-crystalline $_0H_K$, the magneto-elastic $_0H$ and the shape $_0H_{SH}$ anisotropy fields; the temperature and/or composition dependences of the crystalline anisotropy, the saturation magnetostriction, the saturation polarization and the Curie temperature are estimated using data reported in [8, 36, 37].

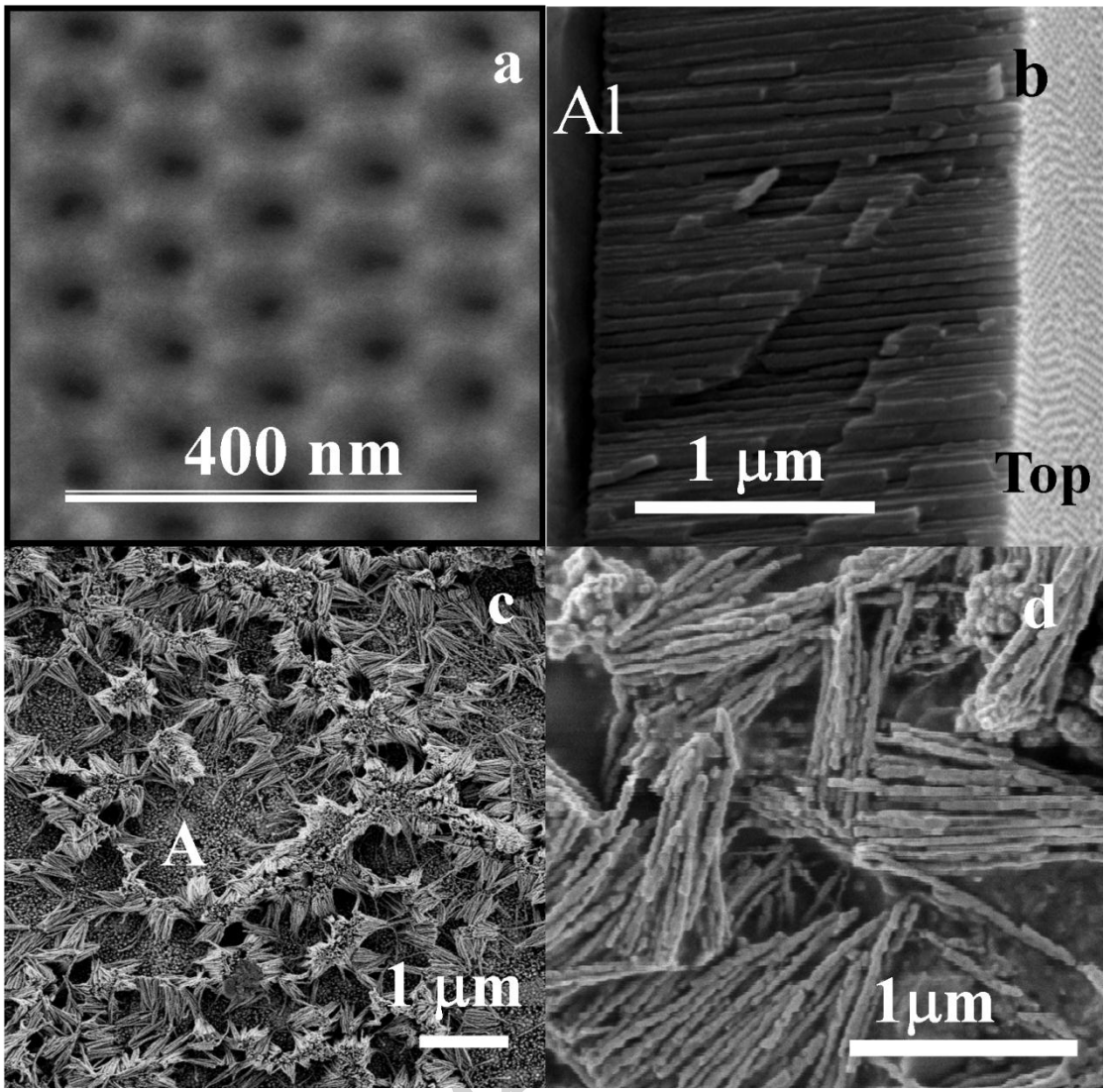

Figure 1. SEM micrographs showing a top view (a) and side view (b) of an alumina template of 26 nm pore diameter, a top view of a template filled by metallic nanowires (c), and nanowires (d), both after the removal of the Al support and a partial dissolution of the alumina template.

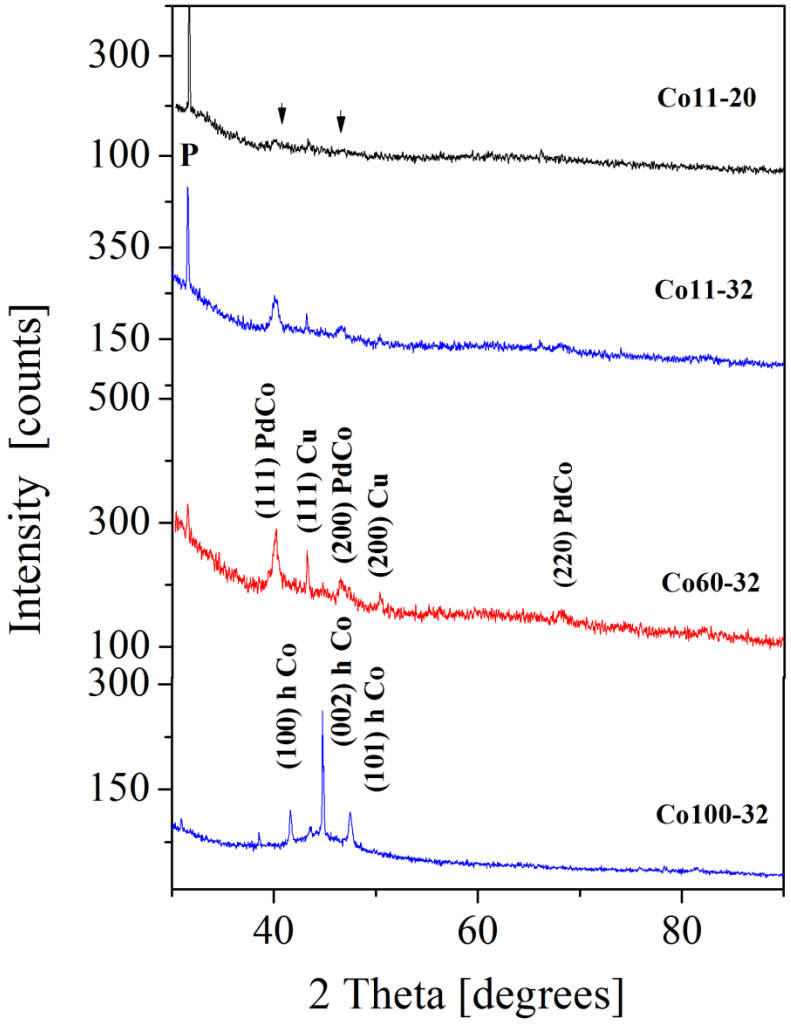

Figure 2. XRD patterns corresponding to arrays Co11-20, Co11-32 and Co60-32 after removal of the Al substrate. The diffractogram corresponding to a Co sample is also included. The reflection denoted by P arises from the polystyrene layer added to improve the membrane mechanical resistance. Small Cu crystals, originated in the Al dissolution process are also detected. The PdCo diffraction lines from the nanowires are hardly detected in Pd-rich samples with 20 nm pore diameter.

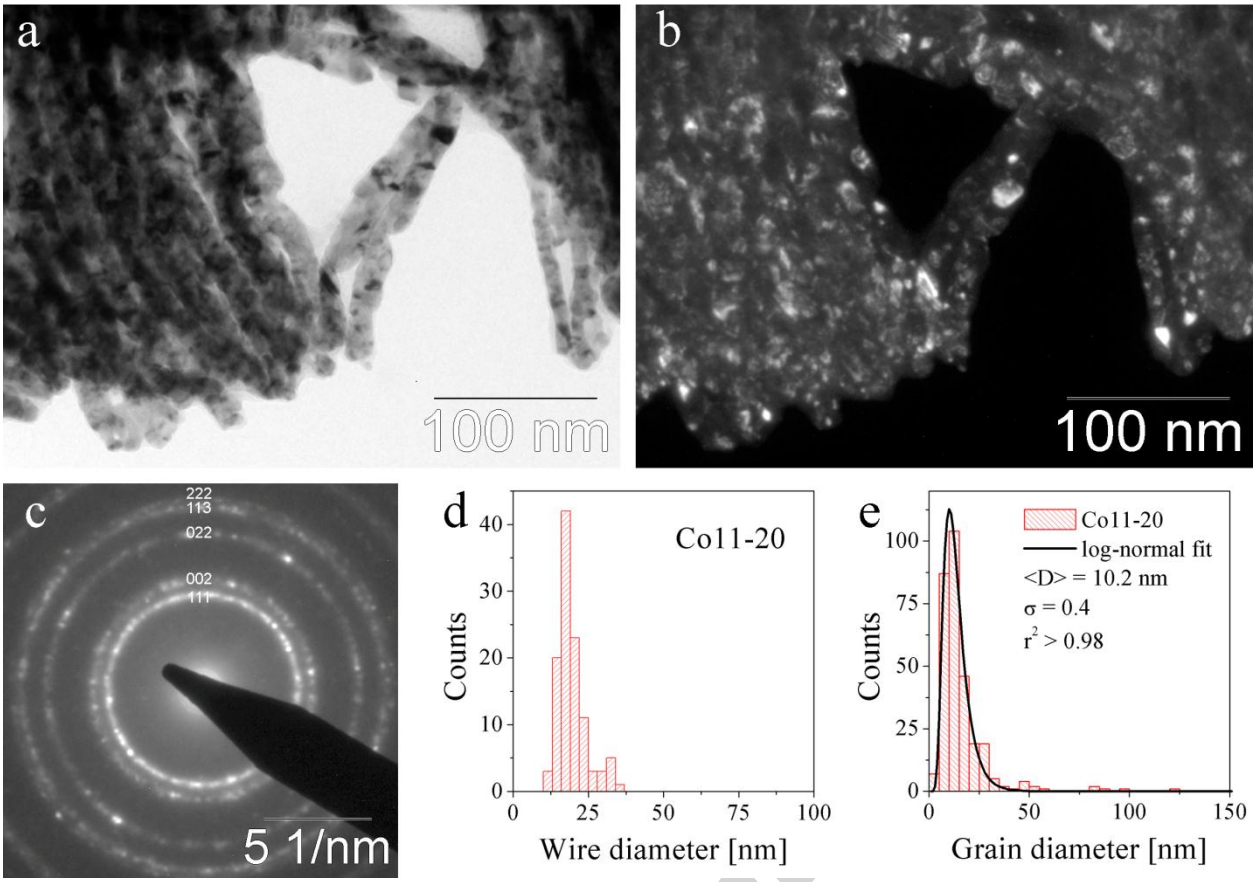

Figure 3. (a) Bright field (BF) TEM micrographs of Co11-20 nanowires; (b) 111 dark field (DF) image illustrating the nanowire internal structure and (c) selected area electron diffraction pattern (SAEDP) corresponding to the nanowires in (a) and (b). Nanowires are polycrystalline, with a quite small grain size. Histograms corresponding to the wire diameter (d) and the grain size (e) distributions resulting from TEM data are included.

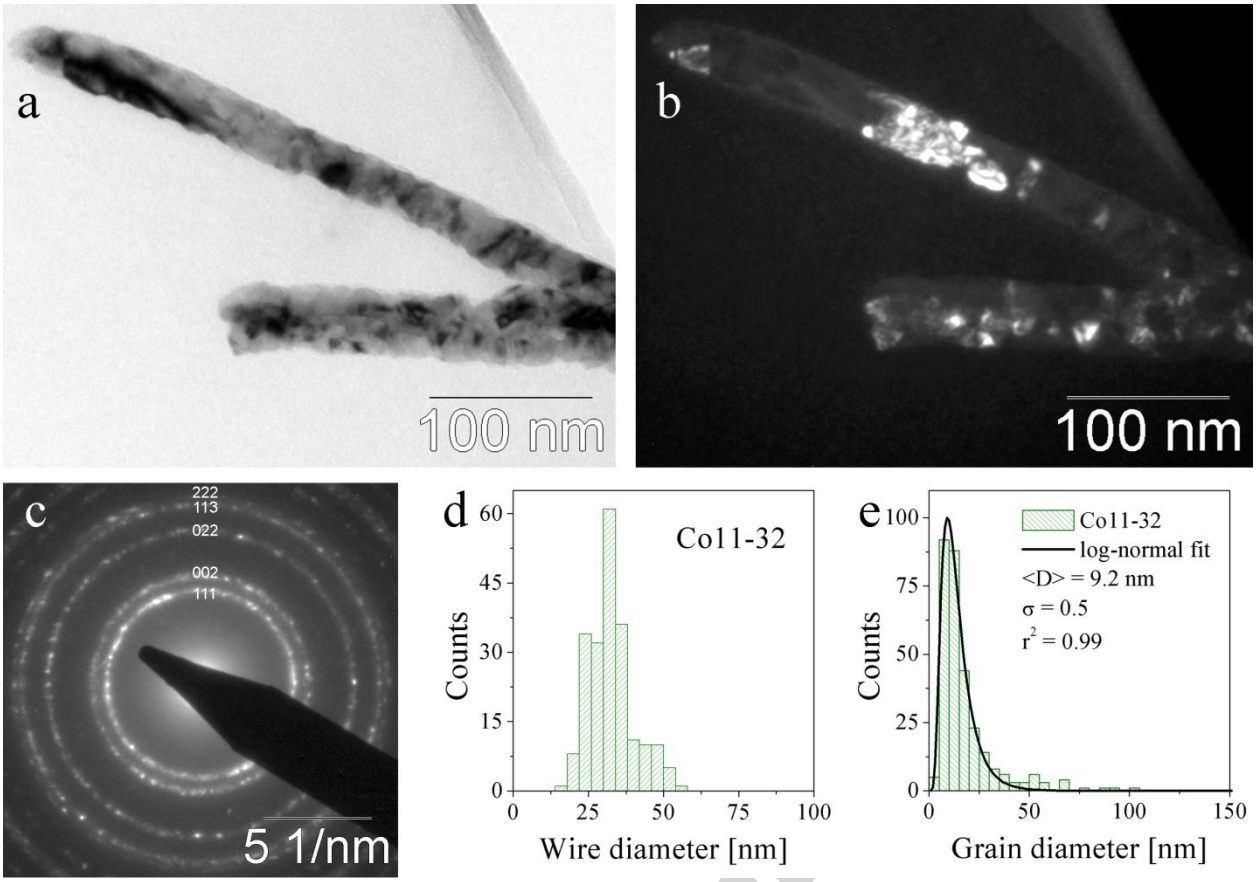

Figure 4. (a) BF TEM micrograph showing Co11-32 nanowires; the corresponding 111 DF image and the SAEDP are shown in (b) and (c) respectively. The polycrystalline nanowire structure is clearly observed. Histograms corresponding to the wire diameter (d) and the grain size (e) distributions are also shown.

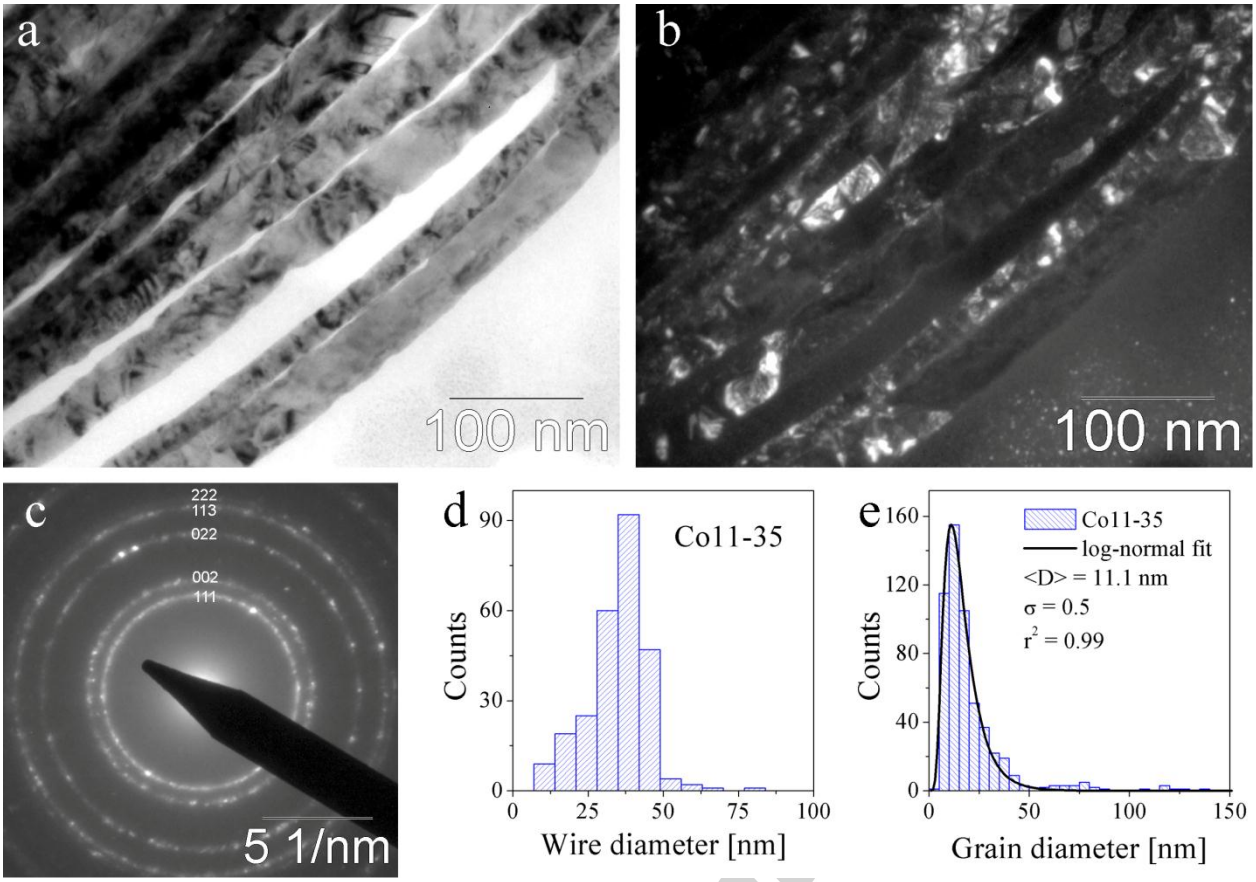

Figure 5. BF TEM micrographs showing Co11-35 nanowires (a); the corresponding 111 DF image (b) and the SAEDP (c) indicate that wires are nanocrystalline. Histograms corresponding to the wire diameter (d) and the grain size (e) distributions are also shown.

.

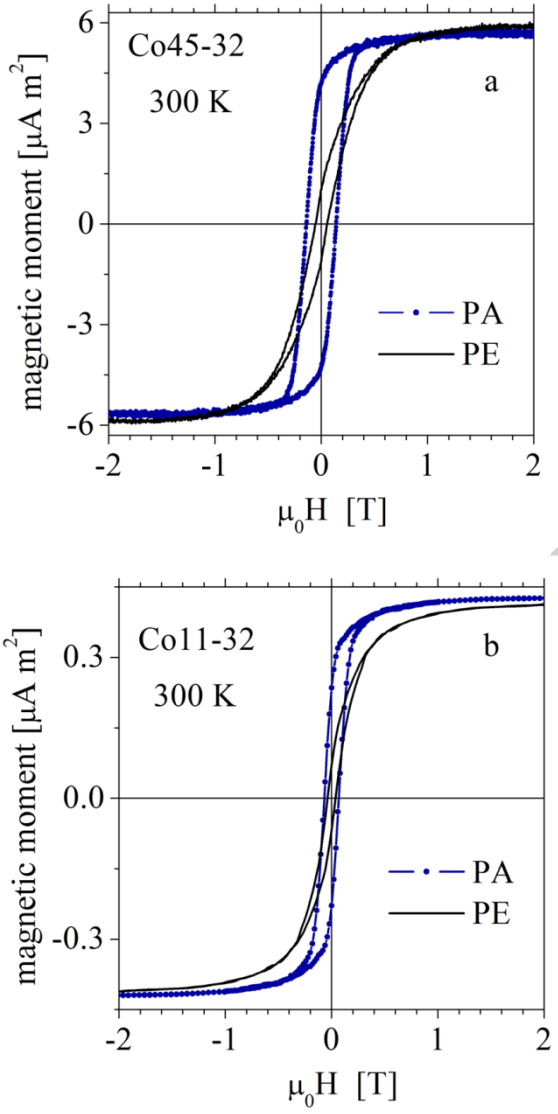

Figure 6. Room temperature hysteresis loops of samples Co45-32 (a) and Co11-32 (b) measured with the applied field parallel (PA) and perpendicular (PE) to the nanowire major axis. The different loops obtained in these two configurations are consistent with relatively large shape anisotropy.

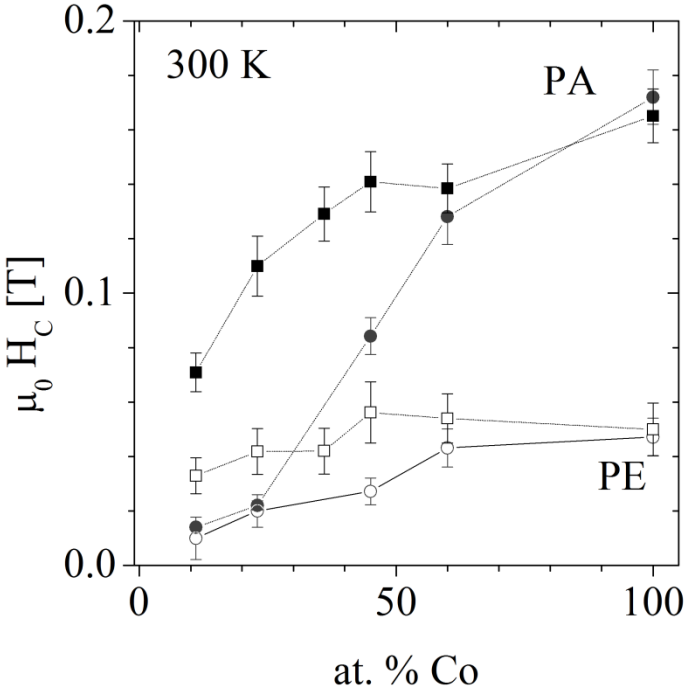

Figure 7. Coercive field as a function of the alloy Co content, in arrays of 26 nm (circles) and 32 nm (squares) diameter nanowires.

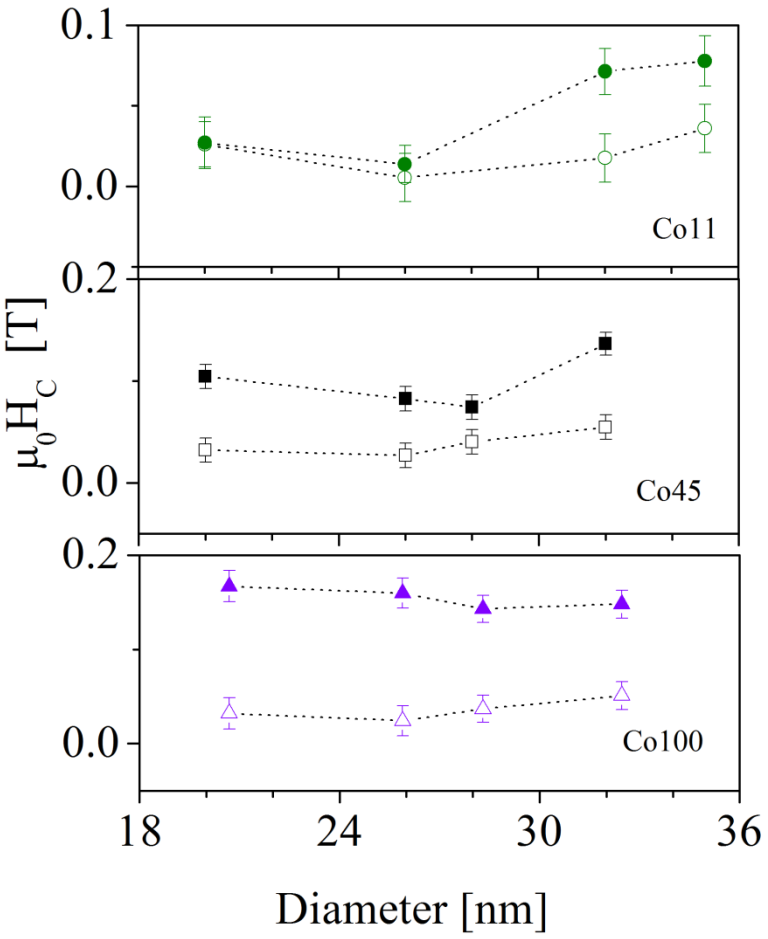

Figure 8. Coercive field as a function of the mean nanowire diameter for arrays with different compositions: pure Co (Co100), $Co_{45}Pd_{55}$ (Co45) and $Co_{11}Pd_{89}$ (Co11). Full symbols correspond to measurements performed with the applied field parallel to the wire long axis while the open ones correspond to the perpendicular configuration.

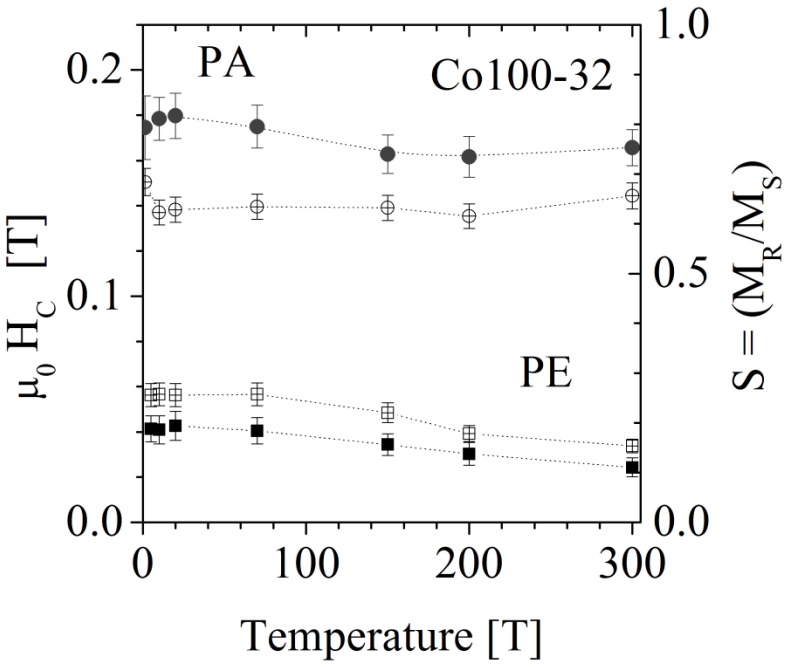

Figure 9. Temperature dependence of coercivity (solid symbols) and squareness (open symbols) in Co nanowire arrays 32 nm in diameter. PA and PE indicate that the magnitude is measured with the magnetic field applied parallel or perpendicular to the nanowire long axis.

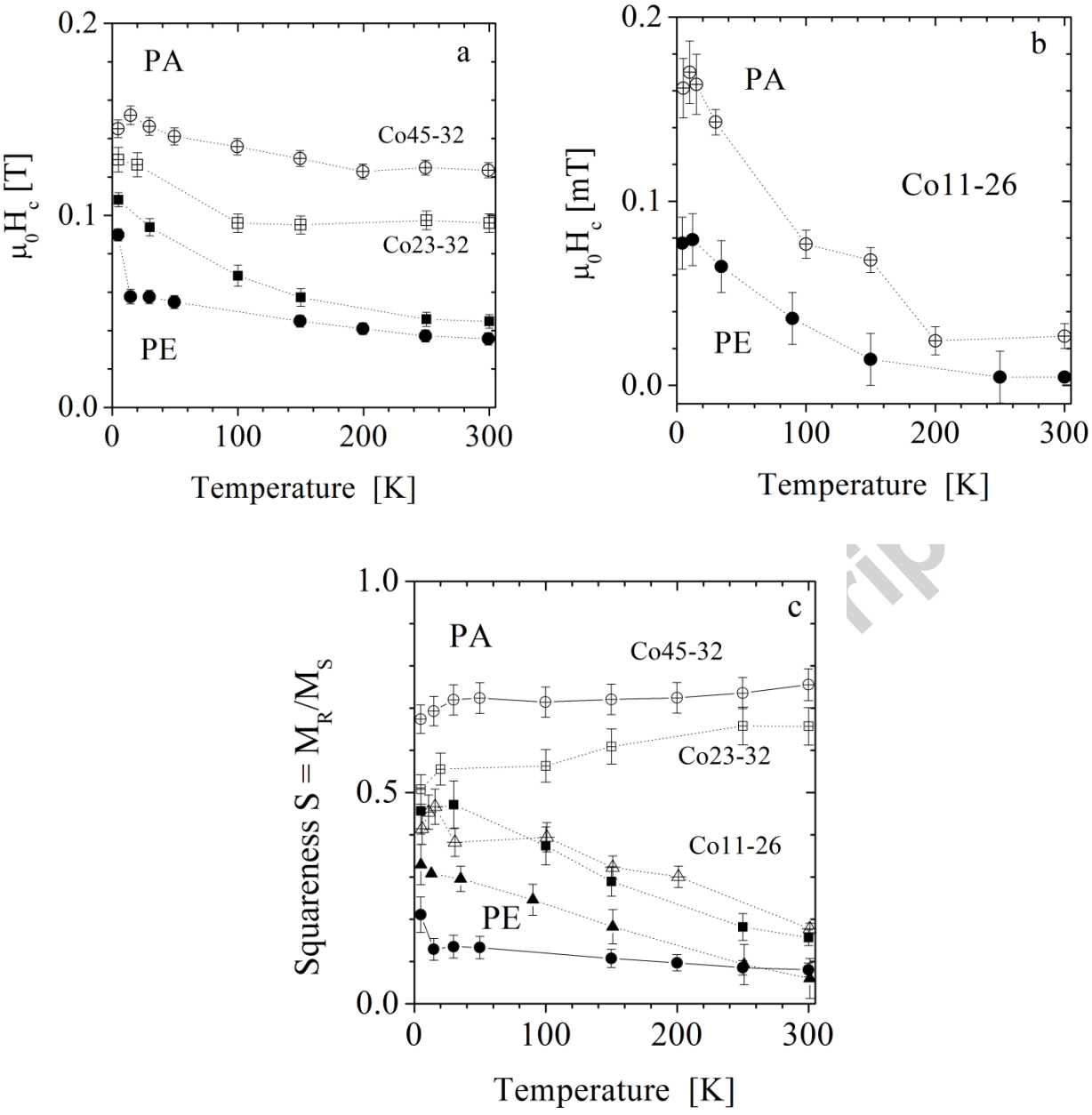

Figure 10. Temperature dependence of coercivity (a and b) and squareness (c) in nanowire arrays with different compositions. PA and PE indicate that the magnitude is measured with the magnetic field applied parallel or perpendicular to the nanowire long axis.

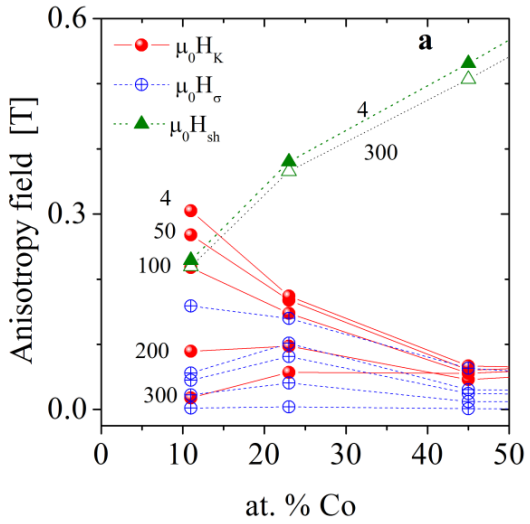

Figure 11. Temperature dependence of the magneto-crystalline $_0H_K$, the magneto-elastic $_0H$ and the shape $_0H_{SH}$ anisotropy fields; the temperature and/or composition dependences of the crystalline anisotropy, the saturation magnetostriction, the saturation polarization and the Curie temperature are estimated using data reported in [8, 35, 36].

Research Highlights

- Polycrystalline Co-Pd nanowires, 20-35nm diameter , 5-12 nm grain size are synthesized.
- Coercivity (14-80 mT) and squareness mainly depend on composition and grain size.
- Different contributions to the effective anisotropy are considered.
- Strong temperature and composition dependence of the nucleation localization is found.

****